62 (2017) APPLICATIONS OF MATHEMATICS No. 1, 75–100

# A NEW ERROR CORRECTION METHOD FOR THE STATIONARY NAVIER-STOKES EQUATIONS BASED ON TWO LOCAL GAUSS INTEGRATIONS

Yun-Bo Yang, Qiong-Xiang Kong, Xi'an

(Received April 17, 2016)

*Abstract.* A new error correction method for the stationary Navier-Stokes equations based on two local Gauss integrations is presented. Applying the orthogonal projection technique, we introduce two local Gauss integrations as a stabilizing term in the error correction method, and derive a new error correction method. In both the coarse solution computation step and the error computation step, a locally stabilizing term based on two local Gauss integrations is introduced. The stability and convergence of the new error correction algorithm are established. Numerical examples are also presented to verify the theoretical analysis and demonstrate the efficiency of the proposed method.

*Keywords*: Navier-Stokes equation; finite element method; variational multiscale; two local Gauss integrations; error correction method

*MSC 2010*: 65N15, 65N30, 65N12

## 1. Introduction

The Navier-Stokes equations provide a mathematical model of an incompressible Newtonian viscous fluid. It can describe many physical phenomena such as indoor air flow, weather variations, flow around airfoils. Therefore, it is very important in studying the efficient numerical methods for the Navier-Stokes equations, see more details in [9], [25], [6]. However, it is well known that the classical finite element method may fail for the Navier-Stokes equations at high Reynolds number and may exhibit global spurious oscillations and yield inaccurate approximation. The reason for this is essentially the dominance of the convection [7], [24]. So some stabilized

This work was supported by the Natural Science Foundation of China (NSFC) under grant no. 11371287, 61663043 and the Natural Science Basic Research Plan in Shaanxi Province of China under grant no. 2016JM5077.

DOI: 10.21136/AM.2017.0119-16 

methods for the simulation of the Navier-Stokes equations at high Reynolds number were proposed; for example, in [29], the artificial viscosity method (AV) adds an artificial viscosity to the inverse Reynolds number as a stabilization factor. The variational multiscale method (VMS) is based on the decomposition of the flow scales and defines the large scales by projection into appropriate subspaces, see [16], [15], [17], [8] for more details. The defect correction method (DCM) for the Navier-Stokes equations at high Reynolds number was proposed, which first solves a nonlinear system and gets a coarse solution in a relative coarse grid, and then obtains a fine solution by solving a linear system in the same grid. It is very efficient, see for example, [20], [3] for the steady Navier-Stokes equations and [18] for the unsteady Navier-Stokes equations. A stabilized finite element method based on two local Gauss integrations was first proposed for the Stokes problem in [21], where the authors applied it to overcome the inf-sup condition restriction between the velocity and pressure. In [28], the authors proved the equivalence of the classical variational multiscale method and the variational multiscale method based on two local Gauss integrations (TGVMS). In [23], the authors combine the two-level method with the defect correction method to solve the Navier-Stokes equations at high Reynolds number. A two-level variational multiscale method for the Navier-Stokes equations based on two local Gauss integrations was presented in [22]. A new defect correction method based on the two-level method was proposed in [13]. In [26], the authors proposed the error correction method (EC) to solve the Navier-Stokes equations at high Reynolds number which can keep a rapid rate of convergence.

The significant feature of our method is that we add a stabilization term based on two local Gauss integrations in both the coarse solution computation step and the error computation step in the error correction method [26]. Compared with other stabilized methods, the stabilization term in our method leads to computing locally at element level, and it is not necessary to introduce any extra variables. It reduces the degrees of freedom of the discrete system, and thus it can save storage. Under the appropriate choice of the stabilization parameter, this method is computationally cheaper than the other methods, and we only need relatively coarse grid to solve the Navier-Stokes equations at high Reynolds number, which can reduce the cost of computation. The numerical examples illustrate that the proposed method is very efficient.

The article is organized as follows. In Section 2, the governing equations together with some notation and some well-known results used throughout this article are given. In Section 3, a new error correction algorithm based on two local Gauss integrations and its stability and error analysis are presented. A series of numerical examples is also given to validate the theoretical analysis and demonstrate the efficiency of our method in Section 4. Finally, some conclusions are presented.

## 2. Preliminaries

We denote by $(\cdot,\cdot)$ the inner product on $L^2(\Omega)$ or $L^2(\Omega)^{d\times d}$. The norm in $(L^2(\Omega))^d$ $(d=2,3)$ and in the standard Sobolev space $H^k(\Omega)$ are $\|\cdot\|$ and $\|\cdot\|_k$, respectively.

**2.1. Some results for the Navier-Stokes equations.** Let $\Omega\subset\mathbb{R}^d$ be an open bounded convex polygonal or polyhedral domain with Lipschitz-continuous boundary $\partial\Omega$. We consider the stationary incompressible Navier-Stokes equations

$$\begin{aligned} -\nu\Delta u+(u\cdot\nabla)u+\nabla p&=f \quad \text{in } \Omega,\\ \nabla\cdot u&=0 \quad \text{in } \Omega,\\ u&=0 \quad \text{on } \partial\Omega, \end{aligned} \tag{2.1}$$

which describle a steady flow of the incompressible viscous Newtonian fluid in a bounded domain. Here $u$ is the fluid velocity and $p$ is the fluid pressure, $f$ is the prescribed body force, and $\nu>0$ is the kinematic viscosity. Given a characteristic length scale $L$ and velocity scale $U$, the Reynolds number is defined by $\mathrm{Re}=UL/\nu$.

For the mathematical setting of problem (2.1), we define the function spaces for the velocity $u$ and pressure $p$, respectively: Consider Hilbert spaces

$$\begin{aligned} X&=H_0^1(\Omega)^d=\{v\in H^1(\Omega)^d\colon\ v=0 \text{ on } \Gamma\},\\ M&=L_0^2(\Omega)=\left\{\varphi\in L^2(\Omega)\colon\ \int_\Omega \varphi\,\mathrm{d}x=0\right\},\\ Y&=L^2(\Omega)^d,\\ V&=\{v\in X\colon\ (\varphi,\nabla\cdot v)=0 \quad \forall\,\varphi\in M\}. \end{aligned}$$

The spaces $X$ and $M$ are equipped with the usual $L^2$-scalar product $(\cdot,\cdot)$ and norm $\|\cdot\|$. And the space $H^{-1}(\Omega)$, the dual space of $H_0^1(\Omega)$, is endowed with the negative norm

$$\|f\|_{-1}=\sup_{v\in H_0^1(\Omega)}\frac{(f,v)}{\|\nabla v\|}.$$

Moreover, we define the trilinear form

$$b(u,v,w)=((u\cdot\nabla)v,w)+\frac{1}{2}((\operatorname{div}u)v,w)=\frac{1}{2}((u\cdot\nabla)v,w)-\frac{1}{2}((u\cdot\nabla)w,v),$$

which has the following properties (see [25], [6]),

$$b(u,v,w)=-b(u,w,v) \quad \forall\,u,v,w\in X, \tag{2.2}$$

$$b(u,v,w)\leqslant N\|\nabla u\|\|\nabla v\|\|\nabla w\| \quad \forall\,u,v,w\in X. \tag{2.3}$$

The weak formulation of problem (2.1) reads: Find $(u,p) \in (X,M)$ such that

$$\nu(\nabla u, \nabla v) + b(u,u,v) - (p, \nabla \cdot v) = (f,v), \tag{2.4}$$
$$(\nabla \cdot u, q) = 0,$$

for all $(v,q) \in (X,M)$.

We need some assumptions on the domain $\Omega$ as in [25], [6]:

(A1) Assume that $\Omega$ is sufficiently smooth and $g \in H^{k-2}(\Omega)^d$, so that the unique solution $(v,q) \in (X,M)$ of the steady Stokes problem

$$-\Delta v + \nabla q = g, \quad \operatorname{div} v = 0 \quad \text{in } \Omega, \quad v|_{\partial\Omega} = 0$$

exists and satisfies

$$\|v\|_k + \|q\|_{k-1} \leqslant c\|g\|_{k-2}, \quad k = 2,3.$$

**Theorem 2.1** (see [25], [6]). *Given $f \in X'$, if the assumption* (A1) *holds, then there exists at least one solution pair $(u,p) \in (X,M)$ which satisfies* (2.4) *and*

$$\|\nabla u\| \leqslant \frac{\|f\|_{-1}}{\nu}, \quad \|p\| \leqslant c\|f\|_{-1}. \tag{2.5}$$

*If $\nu$ and $f$ satisfy the uniqueness condition*

$$\frac{N\|f\|_{-1}}{\nu^2} < 1, \tag{2.6}$$

*then the solution of* (2.4) *is unique.*

**2.2. Finite element approximation.** Let $\tau_h$ be a regular, conforming mesh of $\Omega$ with maximum element diameter $h$. We use the classical Taylor-Hood FE [9] for the approximation in the space of $(u,p)$: $P2$-continuous in velocity, $P1$-continuous in pressure. The corresponding FE spaces are

$$X_h = \{v \in X \cap C^0(\Omega)^d \colon\ v|_K \in P_2(K)^d \quad \forall\, K \in \tau_h\},$$
$$M_h = \{q \in M \cap C^0(\Omega) \colon\ q|_K \in P_1(K) \quad \forall\, K \in \tau_h\},$$

which satisfy the discrete LBB condition

$$\inf_{q_h \in M_h} \sup_{v_h \in X_h} \frac{(q_h, \nabla \cdot v_h)}{\|q_h\|\|\nabla v_h\|} \geqslant \beta > 0. \tag{2.7}$$

Further, the space of weakly divergence-free functions is defined by

$$V_h = \{v_h \in X_h \colon\ (\nabla \cdot v_h, q_h) = 0 \quad \forall\, q_h \in M_h\}. \tag{2.8}$$

Let $u_h$, $p_h$ be the finite element solutions of the Navier-Stokes equations. The finite element approximation of the Navier-Stokes equations is: Find $(u_h, p_h) \in (X_h, M_h)$ such that for all $(v_h, q_h) \in (X_h, M_h)$

$$\begin{gathered}\nu(\nabla u_h, \nabla v_h) + b(u_h, u_h, v_h) - (p_h, \nabla \cdot v_h) = (f, v_h),\\ (\nabla \cdot u_h, q_h) = 0.\end{gathered} \tag{2.9}$$

We also need the space of piecewise constant functions

$$R_0 = \{v_h \in L^2(\Omega) \colon\ v_h|_K \in P_0(K) \quad \forall\, K \in \tau_h\},$$

and define

$$R_h = R_0^{d\times d}.$$

Assume that the couple finite element space $(X_h, M_h)$ satisfies the following approximation properties [25], [6]:

(A2) For each $v \in H^k(\Omega)^2 \cap V$ and $q \in H^{k-1}(\Omega) \cap M$, there exist approximations $\pi_h v \in X_h$, $\varrho_h q \in M_h$ such that

$$\|\nabla(v - \pi_h v)\| \leqslant c h^{k-1} \|v\|_k, \quad \|q - \varrho_h q\| \leqslant c h^{k-1} \|q\|_{k-1}, \quad k = 2, 3. \tag{2.10}$$

In addition, we also assume that the mesh is sufficiently regular so that the inverse inequality holds [1]:

$$\|\nabla v_h\| \leqslant C h^{-1} \|v_h\| \quad \forall\, v_h \in X_h. \tag{2.11}$$

**2.3. Two local Gauss integrations.** The stabilization term is defined by the difference between two local Gauss integrations

$$G(u_h, v_h) = \alpha \sum_K \biggl\{ \int_{K,r} \nabla u_h \cdot \nabla v_h \,\mathrm{d}x - \int_{K,1} \nabla u_h \cdot \nabla v_h \,\mathrm{d}x \biggr\}; \tag{2.12}$$

here $\int_{K,s}(\cdot)\,\mathrm{d}x$ denotes an appropriate Gauss integral on the element $K$, which is exact for polynomials of degree $s$ (here $s = r$, 1 with $r \geqslant 2$), $\alpha > 0$ is a user-defined stabilization parameter. It is equivalent to the stabilized term in the common variational multiscale method; for more details, the reader can see [28], [21]. We introduce

the standard $L^2$-orthogonal projection $\Pi_h\colon\ L^2(\Omega)^{d\times d} \to R_h$ with the following properties:

$$(\Pi_h \nabla u, v) = (\nabla u, v) \quad \forall\, u \in X, v \in R_h, \tag{2.13}$$

$$\|\Pi_h \nabla v\| \leqslant \|\nabla v\| \quad \forall\, v \in X. \tag{2.14}$$

Noting that we can choose $r$ such that the first Gauss integration in (2.12) is exactly that of $\int_K \nabla u_h \cdot \nabla v_h \,\mathrm{d}x$ on the element $K$, we can rewrite the stabilization term (2.12) as

$$G(u_h, v_h) = \alpha(\nabla u_h, \nabla v_h) - \alpha(\Pi_h \nabla u_h, \nabla v_h), \tag{2.15}$$

which has the property

$$G(u_h, v_h) \leqslant 2\alpha \|\nabla u_h\| \|\nabla v_h\|. \tag{2.16}$$

## 3. Error correction method based on two local Gauss integrations

As mentioned earlier, the standard Galerkin finite element method for (2.4) may fail due to the dominance of convection. Therefore, stabilized methods are required. We first recall the classical variational multiscale method (VMS), which was proposed in [19], [16] for the stationary Navier-Stokes equations. Denote two spaces by $L = L^2(\Omega)^{d\times d}$ and $L_h \subset L$. The VMS method is determined by the choices of $L_h$ and the stabilization parameter $\alpha$. There are different choices of selecting $L_h$, which lead to different VMS methods. One case is choosing $L_h = R_h$, which is defined on the same grid as $X_h$. Then, the classical VMS method is: Find $(u_h, p_h) \in (X_h, M_h)$, $g_h \in L_h$ satisfying

$$\begin{aligned} (\nu+\alpha)(\nabla u_h, \nabla v_h) - \alpha(g_h, \nabla v_h) + b(u_h, u_h, v_h) - (p_h, \nabla \cdot v_h) & \\ = (f, v_h) \quad \forall\, v_h \in X_h, & \\ (\nabla \cdot u_h, q_h) = 0 \quad \forall\, q_h \in M_h, & \\ (g_h - \nabla u_h, l_h) = 0 \quad \forall\, l_h \in L_h. & \end{aligned} \tag{3.1}$$

Besides, the stabilization parameter $\alpha$ in this method acts only on small scales. Although the VMS method above has been shown to preserve stability and high efficiency, the extra storage might be significant, since it introduces four additional variables in the two-dimensional case and nine additional variables in the three-dimensional case. In [28], the authors proposed a very efficient method to reduce

the extra storage without introducing any additional variables. After defining the standard $L^2$-orthogonal projection $\Pi_h\colon\ L^2(\Omega)^{d\times d} \to R_h$ with properties (2.13) and (2.14), we can rewrite system (3.1) as

$$\begin{aligned}(3.2)\qquad \nu(\nabla u_h, \nabla v_h) + \alpha((\mathbf{I}-\Pi_h)\nabla u_h, (\mathbf{I}-\Pi_h)\nabla v_h) + b(u_h, u_h, v_h)& \\ -(p_h, \nabla\cdot v_h) = (f, v_h) \quad \forall\, v_h \in X_h,& \\ (\nabla\cdot u_h, q_h) = 0 \quad \forall\, q_h \in M_h,&\end{aligned}$$

where $\mathbf{I}$ denotes the identity operator.

As discussed in [28], system (3.2) has an equivalent version based on two local Gauss integrations: Find $(u_h, p_h) \in (X_h, M_h)$ such that

$$\begin{aligned}(3.3)\ \nu(\nabla u_h, \nabla v_h) + G(u_h, v_h) + b(u_h, u_h, v_h) - (p_h, \nabla\cdot v_h) = (f, v_h) \quad \forall\, v_h \in X_h,& \\ (\nabla\cdot u_h, q_h) = 0 \quad \forall\, q_h \in M_h.&\end{aligned}$$

For this stabilization method (3.3), some results have been given, and we recall them in the following theorem.

**Theorem 3.1** ([11], [14]). *Let the exact solution $(u, p)$ of (2.4) be in $(H^3(\Omega)^d \cap X$, $H^2(\Omega)\cap M)$. Then the solution $(u_h, p_h)$ of (3.3) satisfies the stability and error estimates*

$$(3.4)\qquad \|\nabla u_h\| \leqslant \frac{\|f\|_{-1}}{\nu},$$

$$(3.5)\qquad \nu\|u-u_h\| + h(\nu\|\nabla(u-u_h)\| + \|p-p_h\|) \leqslant ch^3(\nu\|u\|_3 + \|p\|_2).$$

We can choose the Oseen iteration to solve (3.3) as follows (see [10]):

$$\begin{aligned}(3.6)\quad \nu(\nabla u_h^m, \nabla v_h) + G(u_h^m, v_h) + b(u_h^{m-1}, u_h^m, v_h) - (p_h^m, \nabla\cdot v_h) = (f, v_h),& \\ (\nabla\cdot u_h^m, q_h) = 0.&\end{aligned}$$

Here $(u_h^0, p_h^0) \in (X_h, M_h)$ is solved by

$$\begin{aligned}(3.7)\qquad \nu(\nabla u_h^0, \nabla v_h) + G(u_h^0, v_h) - (p_h^0, \nabla\cdot v_h) = (f, v_h),& \\ (\nabla\cdot u_h^0, q_h) = 0.&\end{aligned}$$

Supposing that $u_h^{m-1}$ is given, the course solution $(U_h^m, P_h^m)$ is computed by using (3.6) as

$$\begin{aligned}(3.8)\quad \nu(\nabla U_h^m, \nabla v_h) + G(U_h^m, v_h) + b(u_h^{m-1}, U_h^m, v_h) - (P_h^m, \nabla\cdot v_h) = (f, v_h),& \\ (\nabla\cdot U_h^m, q_h) = 0.&\end{aligned}$$

Subtracting (3.8) from (3.3), we get the error equation

$$\nu(\nabla\varepsilon_h^m,\nabla v_h)+G(\varepsilon_h^m,v_h)+b(u_h,u_h,v_h)-b(u_h^{m-1},U_h^m,v_h)-(\theta_h^m,\nabla\cdot v_h)=0, \tag{3.9}$$
$$(\nabla\cdot\varepsilon_h^m,q_h)=0,$$

where $\varepsilon_h^m=u_h-U_h^m$, $\theta_h^m=p_h-P_h^m$.

With simple calculation, we get

$$\begin{aligned} &b(u_h,u_h,v_h)-b(u_h^{m-1},U_h^m,v_h)\\ &\quad=b(u_h,u_h,v_h)-b(u_h,U_h^m,v_h)+b(u_h,U_h^m,v_h)-b(u_h^{m-1},U_h^m,v_h)\\ &\quad=b(u_h,\varepsilon_h^m,v_h)+b(u_h-u_h^{m-1},U_h^m,v_h)\\ &\quad=b(\varepsilon_h^m+U_h^m,\varepsilon_h^m,v_h)+b(\varepsilon_h^m+U_h^m,U_h^m,v_h)-b(u_h^{m-1},U_h^m,v_h)\\ &\quad=b(\varepsilon_h^m,\varepsilon_h^m,v_h)+b(U_h^m,\varepsilon_h^m,v_h)+b(\varepsilon_h^m,U_h^m,v_h)\\ &\qquad+b(U_h^m,U_h^m,v_h)-b(u_h^{m-1},U_h^m,v_h). \end{aligned} \tag{3.10}$$

Replacing $b(\varepsilon_h^m,\varepsilon_h^m,v_h)$ by $b(\varepsilon_h^{m-1},\varepsilon_h^m,v_h)$ in the RHS of (3.10), the error correction algorithm based on two local Gauss integrations (TGEC) for solving the stationary Navier-Stokes equations is derived as follows:

**Algorithm** (TGEC):

*Step 1.* Given $(u_h^0,p_h^0)$, find a relative coarse solution $(U_h^m,P_h^m)\in(X_h,M_h)$ by the scheme

$$\nu(\nabla U_h^m,\nabla v_h)+G(U_h^m,v_h)+b(u_h^{m-1},U_h^m,v_h)-(P_h^m,\nabla\cdot v_h)=(f,v_h), \tag{3.11}$$
$$(\nabla\cdot U_h^m,q_h)=0.$$

*Step 2.* Find the error $(\varepsilon_h^m,\theta_h^m)\in(X_h,M_h)$ by the scheme

$$\begin{aligned} &\nu(\nabla\varepsilon_h^m,\nabla v_h)+G(\varepsilon_h^m,v_h)+b(\varepsilon_h^{m-1},\varepsilon_h^m,v_h)+b(U_h^m,\varepsilon_h^m,v_h)\\ &\quad+b(\varepsilon_h^m,U_h^m,v_h)+b(U_h^m,U_h^m,v_h)-b(u_h^{m-1},U_h^m,v_h)-(\theta_h^m,\nabla\cdot v_h)=0,\\ &\qquad(\nabla\cdot\varepsilon_h^m,q_h)=0. \end{aligned} \tag{3.12}$$

*Step 3.* Set $u_h^m=U_h^m+\varepsilon_h^m$, $p_h^m=P_h^m+\theta_h^m$. If the stopping criterion is satisfied, stop. Else, set $m=m+1$, go to step 1.

R e m a r k 3.1. Our algorithm is based on two local Gauss integrations. It is different from the error correct algorithm (EC) in [26], since in each step, a locally stabilized technique based on the Gaussian quadrature rule is used. This allows to solve the stationary Navier-Stokes equations at high Reynolds number on a relatively coarse grid, and to reduce the cost of computation. Our numerical experiments in Section 4 will verify this good property.

R e m a r k 3.2. The initial value $(u_h^0, p_h^0) \in (X_h, M_h)$ of TGEC algorithm is chosen by solving problem (3.7) and we set $U_h^0 = u_h^0$, $P_h^0 = p_h^0$.

We first give the stability estimates of TGEC algorithm in the following theorem.

**Theorem 3.2.** *Given $f \in X'$, if the assumptions* (A1), (A2) *and the uniqueness condition* (2.6) *hold, then we have*

$$\|\nabla U_h^m\| \leqslant \frac{\|f\|_{-1}}{\nu} \tag{3.13}$$

*and*

$$\|\nabla u_h^m\| \leqslant \frac{3}{\mu}\|f\|_{-1} + \frac{2\alpha}{\nu\mu}\|f\|_{-1} + \frac{1}{\nu}\|f\|_{-1}, \tag{3.14}$$

*where $\mu = \nu - N\|f\|_{-1}/\nu$.*

P r o o f. Taking $(v_h, q_h) = (U_h^m, P_h^m) \in (V_h, M_h)$ in (3.11) and using (2.2), (2.8), (2.14), and (2.15), we get

$$\begin{aligned}(\nu+\alpha)\|\nabla U_h^m\|^2 &= (f, U_h^m) + \alpha(\Pi_h \nabla U_h^m, \nabla U_h^m) \\ &\leqslant \|f\|_{-1}\|\nabla U_h^m\| + \alpha\|\Pi_h \nabla U_h^m\|\|\nabla U_h^m\| \\ &\leqslant \|f\|_{-1}\|\nabla U_h^m\| + \alpha\|\nabla U_h^m\|^2.\end{aligned} \tag{3.15}$$

Then estimate (3.13) follows obviously.

Next, setting $v_h = \varepsilon_h^m$ in (3.12), by virtue of (2.2) and (2.8), we arrive at

$$\begin{aligned}\nu\|\nabla \varepsilon_h^m\|^2 + G(\varepsilon_h^m, \varepsilon_h^m) + b(\varepsilon_h^m, U_h^m, \varepsilon_h^m) \\ + b(U_h^m, U_h^m, \varepsilon_h^m) - b(u_h^{m-1}, U_h^m, \varepsilon_h^m) = 0.\end{aligned} \tag{3.16}$$

Taking $v_h = \varepsilon_h^m$ in (3.11), we obtain

$$\nu(\nabla U_h^m, \nabla \varepsilon_h^m) + G(U_h^m, \varepsilon_h^m) + b(u_h^{m-1}, U_h^m, \varepsilon_h^m) = (f, \varepsilon_h^m). \tag{3.17}$$

Adding (3.16) and (3.17) yields

$$\begin{aligned}\nu\|\nabla \varepsilon_h^m\|^2 + \nu(\nabla U_h^m, \nabla \varepsilon_h^m) + G(\varepsilon_h^m, \varepsilon_h^m) + G(U_h^m, \varepsilon_h^m) \\ + b(\varepsilon_h^m, U_h^m, \varepsilon_h^m) + b(U_h^m, U_h^m, \varepsilon_h^m) = (f, \varepsilon_h^m).\end{aligned} \tag{3.18}$$

Making use of (2.3), (2.14), (2.15), (2.16), and the Cauchy-Schwarz inequality in (3.18), we get

$$\begin{aligned}\nu\|\nabla \varepsilon_h^m\|^2 \leqslant \nu\|\nabla U_h^m\|\|\nabla \varepsilon_h^m\| + N\|\nabla U_h^m\|\|\nabla \varepsilon_h^m\|^2 + N\|\nabla U_h^m\|^2\|\nabla \varepsilon_h^m\| \\ + 2\alpha\|\nabla U_h^m\|\|\nabla \varepsilon_h^m\| + \|f\|_{-1}\|\nabla \varepsilon_h^m\|.\end{aligned} \tag{3.19}$$

Using (3.13) and the uniqueness condition (2.6) in (3.19) yields

$$\|\nabla\varepsilon_h^m\| \leqslant \frac{3}{\mu}\|f\|_{-1} + \frac{2\alpha}{\mu\nu}\|f\|_{-1},$$

where $\mu = \nu - N\|f\|_{-1}/\nu$. Combining the above inequality with (3.13), with help of the triangle inequality we obtain (3.14). □

Next, we will give the error estimates of TGEC algorithm. To do this, we first establish the error equation of TGEC algorithm. By adding (3.11) and (3.12), we obtain

$$\begin{aligned}(3.20)\qquad \nu(\nabla u_h^m, \nabla v_h) + G(u_h^m, v_h) + b(u_h^m, u_h^m, v_h) + b(\varepsilon_h^{m-1}, \varepsilon_h^m, v_h)\\ -b(\varepsilon_h^m, \varepsilon_h^m, v_h) - (p_h^m, \nabla\cdot v_h) = (f, v_h),\\ (\nabla\cdot u_h^m, q_h) = 0.\end{aligned}$$

Let $e_h^m = u_h - u_h^m$ and $\eta_h^m = p_h - p_h^m$. Then subtracting (3.20) from (3.3) and using the identity

$$b(u_h, u_h, v_h) - b(u_h^m, u_h^m, v_h) = b(u_h, e_h^m, v_h) - b(e_h^m, e_h^m, v_h) + b(e_h^m, u_h, v_h),$$

we arrive at

$$\begin{aligned}(3.21)\qquad \nu(\nabla e_h^m, \nabla v_h) + G(e_h^m, v_h) + b(u_h, e_h^m, v_h) - b(e_h^m, e_h^m, v_h)\\ +b(e_h^m, u_h, v_h) - b(\varepsilon_h^{m-1} - \varepsilon_h^m, \varepsilon_h^m, v_h) - (\eta_h^m, \nabla\cdot v_h) = 0,\\ (\nabla\cdot e_h^m, q_h) = 0.\end{aligned}$$

Let $E_h^m = u_h - U_h^m$ and $\Theta_h^m = p_h - P_h^m$. Then subtracting (3.11) from (3.3) and using the identity

$$\begin{aligned}&b(u_h, u_h, v_h) - b(u_h^{m-1}, U_h^m, v_h)\\ &\quad= b(u_h, u_h, v_h) - b(u_h^{m-1}, u_h, v_h) + b(u_h^{m-1}, u_h, v_h) - b(u_h^{m-1}, U_h^m, v_h)\\ &\quad= b(e_h^{m-1}, u_h, v_h) + b(u_h^{m-1}, E_h^m, v_h),\end{aligned}$$

we obtain

$$\begin{aligned}(3.22)\qquad \nu(\nabla E_h^m, \nabla v_h) + G(E_h^m, v_h) + b(e_h^{m-1}, u_h, v_h) + b(u_h^{m-1}, E_h^m, v_h)\\ -(\Theta_h^m, \nabla\cdot v_h) = 0 \quad \forall\, v_h \in X_h,\\ (\nabla\cdot E_h^m, q_h) = 0 \quad \forall\, q_h \in M_h.\end{aligned}$$

And we can easily get the identity,

$$\varepsilon_h^m = u_h^m - U_h^m = E_h^m - e_h^m. \tag{3.23}$$

Using the error equations (3.21), (3.22), and the identity (3.23), we can obtain the error estimates for our algorithm (TGEC).

**Lemma 3.1.** *Under the assumptions of Theorem* 3.2*, we have*

$$\|\nabla e_h^0\| \leqslant \frac{\|f\|_{-1}}{\nu - 2\alpha} \frac{N\|f\|_{-1}}{\nu^2}. \tag{3.24}$$

P r o o f. Subtracting (3.7) from (3.3), we obtain

$$\begin{gathered} \nu(\nabla e_h^0, \nabla v_h) + G(e_h^0, v_h) + b(u_h, u_h, v_h) - (\eta_h^0, \nabla \cdot v_h) = 0, \\ (\nabla \cdot e_h^0, q_h) = 0. \end{gathered} \tag{3.25}$$

Choosing $(v_h, q_h) = (e_h^0, \eta_h^0) \in (V_h, M_h)$ in (3.25) and using (2.3), (2.16), and the Cauchy-Schwarz inequality, we get

$$\nu\|\nabla e_h^0\|^2 \leqslant 2\alpha\|\nabla e_h^0\|^2 + N\|\nabla u_h\|^2\|\nabla e_h^0\|. \tag{3.26}$$

After using Theorem 3.1, we obtain estimates (3.24). □

**Lemma 3.2.** *Under the assumptions of Theorem* 3.2*, for $m \geqslant 1$, if $\nu$ and $f$ satisfy the condition*

$$\left(\frac{N\|f\|_{-1}}{\nu^2}\right)^{3m-7} \left(1 + \left(\frac{N\|f\|_{-1}}{\nu^2}\right)^3 + \left(\frac{N\|f\|_{-1}}{\nu^2}\right)^2\right) \leqslant \mu - 2\alpha,$$

*where $\mu = \nu - N\|f\|_{-1}/\nu$ as previously, the solution of the TGEC algorithm satisfies*

$$\|\nabla e_h^m\| \leqslant c\left(\frac{N\|f\|_{-1}}{\nu^2}\right)^{3m} \tag{3.27}$$

*and*

$$\|\nabla E_h^m\| \leqslant c\left(\frac{N\|f\|_{-1}}{\nu^2}\right)^{3m-2}, \tag{3.28}$$

*where $c = c(\nu, \alpha, f, \Omega)$ is an appropriate constant, which is independent of the mesh parameter, and may take on different values at different places.*

P r o o f. We prove the theorem by the inductive method. For $m = 1$, the conclusion holds. In fact, setting $m = 1$ and $(v_h, q_h) = (E_h^1, \theta_h^1) \in (V_h, M_h)$ in (3.22), we arrive at

$$\nu\|\nabla E_h^1\|^2 + G(E_h^1, E_h^1) + b(e_h^0, u_h, E_h^1) = 0. \tag{3.29}$$

By using (2.3) and (2.16), we obtain

$$\nu\|\nabla E_h^1\|^2 \leqslant 2\alpha\|\nabla E_h^1\|^2 + N\|\nabla e_h^0\|\|\nabla u_h\|\|\nabla E_h^1\|. \tag{3.30}$$

Applying Theorem 3.1, Lemma 3.1, and the uniqueness condition (2.6), we get

$$\|\nabla E_h^1\| \leqslant \frac{N}{\nu - 2\alpha}\frac{\|f\|_{-1}}{v - 2\alpha}\frac{N\|f\|_{-1}}{\nu^2}\frac{\|f\|_{-1}}{\nu} \leqslant \frac{\nu\|f\|_{-1}}{(\nu - 2\alpha)^2}\frac{N\|f\|_{-1}}{\nu^2}. \tag{3.31}$$

Setting $m = 1$ and $(v_h, q_h) = (e_h^1, \eta_h^1) \in (V_h, M_h)$ in (3.21), and using (2.2) and (3.23), we obtain

$$\nu\|\nabla e_h^1\|^2 + G(e_h^1, e_h^1) + b(e_h^1, u_h, e_h^1) - b(E_h^0 - e_h^0 - E_h^1 + e_h^1, E_h^1, e_h^1) = 0. \tag{3.32}$$

With the help of Theorem 3.2, (2.16), (2.2), and (2.3), we get

$$\begin{aligned}\nu\|\nabla e_h^1\|^2 &= -G(e_h^1, e_h^1) - b(e_h^1, u_h, e_h^1) + b(E_h^0 - e_h^0 - E_h^1 + e_h^1, E_h^1, e_h^1)\\ &= -G(e_h^1, e_h^1) - b(e_h^1, U_h^1, e_h^1) + b(E_h^0 - e_h^0 - E_h^1, E_h^1, e_h^1)\\ &\leqslant 2\alpha\|\nabla e_h^1\|^2 + N\|\nabla U_h^1\|\|\nabla e_h^1\|^2 + N\|\nabla E_h^1\|^2\|\nabla e_h^1\|.\end{aligned} \tag{3.33}$$

Using (3.31), we obtain

$$\begin{aligned}\left(\nu - 2\alpha - \frac{N\|f\|_{-1}}{\nu}\right)\|\nabla e_h^1\| &\leqslant N\left(\frac{\nu\|f\|_{-1}}{(\nu - 2\alpha)^2}\right)^2\left(\frac{N\|f\|_{-1}}{\nu^2}\right)^2\\ &= \frac{\nu^3\|f\|_{-1}}{(\nu - 2\alpha)^4}\left(\frac{N\|f\|_{-1}}{\nu^2}\right)^3\end{aligned} \tag{3.34}$$

which yields

$$\|\nabla e_h^1\| \leqslant \frac{1}{\mu - 2\alpha}\frac{\nu^4\|f\|_{-1}}{(\nu - 2\alpha)^4}\left(\frac{N\|f\|_{-1}}{\nu^2}\right)^3. \tag{3.35}$$

Assume that the estimates (3.27) and (3.28) hold for $1 < k \leqslant m - 1$, namely, $\|\nabla e_h^k\| \leqslant c_1(N\|f\|_{-1}/\nu^2)^{3k}$, $\|\nabla E_h^k\| \leqslant c_2(N\|f\|_{-1}/\nu^2)^{3k-2}$, $k = 2, 3, \ldots, m - 1$. Next, we need to prove that (3.27) and (3.28) also hold for $k = m$.

Taking $(v_h, q_h) = (E_h^m, \theta_h^m) \in (V_h, M_h)$ in (3.22) yields

$$\begin{aligned}\nu\|\nabla E_h^m\|^2 &\leqslant 2\alpha\|\nabla E_h^m\|^2 + N\|\nabla u_h\|\|\nabla e_h^{m-1}\|\|\nabla E_h^m\| \\ &\leqslant 2\alpha\|\nabla E_h^m\|^2 + N\frac{\|f\|_{-1}}{\nu}\|\nabla e_h^{m-1}\|\|\nabla E_h^m\|.\end{aligned} \tag{3.36}$$

Thus

$$\|\nabla E_h^m\| \leqslant \frac{1}{\nu - 2\alpha}\frac{N\|f\|_{-1}}{\nu}\|\nabla e_h^{m-1}\|. \tag{3.37}$$

Inserting the bounds of $\|\nabla e_h^{m-1}\|$ into (3.37) produces

$$\|\nabla E_h^m\| \leqslant \frac{c_1\nu}{\nu - 2\alpha}\left(\frac{N\|f\|_{-1}}{\nu^2}\right)^{3m-2} \leqslant c_1\left(\frac{N\|f\|_{-1}}{\nu^2}\right)^{3m-2}. \tag{3.38}$$

Setting $(v_h, q_h) = (e_h^m, \eta_h^m) \in (V_h, M_h)$ in (3.21), and using (3.23) and (2.2), we obtain

$$\begin{aligned}&\nu\|\nabla e_h^m\|^2 + G(e_h^m, e_h^m) + b(e_h^m, U_h^m, e_h^m) \\ &\qquad - b(E_h^{m-1} - E_h^m, E_h^m, e_h^m) - b(e_h^{m-1}, E_h^m, e_h^m) = 0.\end{aligned} \tag{3.39}$$

So

$$\begin{aligned}\nu\|\nabla e_h^m\|^2 &\leqslant 2\alpha\|\nabla e_h^m\|^2 + N\|\nabla e_h^m\|^2\|\nabla U_h^m\| \\ &\quad + N(\|\nabla E_h^{m-1}\| + \|\nabla E_h^m\|)\|\nabla E_h^m\|\|\nabla e_h^m\| \\ &\quad + N\|\nabla e_h^{m-1}\|\|\nabla E_h^m\|\|\nabla e_h^m\|.\end{aligned} \tag{3.40}$$

Inserting the bounds of $\|\nabla e_h^{m-1}\|$, $\|\nabla E_h^{m-1}\|$ and $\|\nabla E_h^m\|$ into (3.40), we get

$$\begin{aligned}&\left(\nu - 2\alpha - \frac{N\|f\|_{-1}}{\nu}\right)\|\nabla e_h^m\| \\ &\quad\leqslant N(\|\nabla E_h^{m-1}\| + \|\nabla E_h^m\|)\|\nabla E_h^m\| + N\|\nabla e_h^{m-1}\|\|\nabla E_h^m\| \\ &\quad\leqslant N\left(\|\nabla E_h^{m-1}\| + \frac{1}{\nu - 2\alpha}\frac{N\|f\|_{-1}}{\nu}\|\nabla e_h^{m-1}\|\right)\frac{1}{\nu - 2\alpha}\frac{N\|f\|_{-1}}{\nu}\|\nabla e_h^{m-1}\| \\ &\qquad + \frac{N}{\nu - 2\alpha}\frac{N\|f\|_{-1}}{\nu}\|\nabla e_h^{m-1}\|^2 \\ &\quad\leqslant N\left(c_2\left(\frac{N\|f\|_{-1}}{\nu^2}\right)^{3m-5} + \frac{c_1}{\nu - 2\alpha}\frac{N\|f\|_{-1}}{\nu}\left(\frac{N\|f\|_{-1}}{\nu^2}\right)^{3m-3}\right) \\ &\qquad\quad \times \frac{c_1}{\nu - 2\alpha}\frac{N\|f\|_{-1}}{\nu}\left(\frac{N\|f\|_{-1}}{\nu^2}\right)^{3m-3} \\ &\qquad + \frac{Nc_1}{\nu - 2\alpha}\frac{N\|f\|_{-1}}{\nu}\left(\frac{N\|f\|_{-1}}{\nu^2}\right)^{6m-6}\end{aligned} \tag{3.41}$$

$$
\begin{aligned}
&\leqslant N\bigg(\frac{c_2\nu}{\nu-2\alpha}\bigg(\frac{N\|f\|_{-1}}{\nu^2}\bigg)^{6m-7}+\frac{c_1\nu^2}{(\nu-2\alpha)^2}\bigg(\frac{N\|f\|_{-1}}{\nu^2}\bigg)^{6m-4}\bigg)\\
&\quad+\frac{N\nu c_1}{\nu-2\alpha}\bigg(\frac{N\|f\|_{-1}}{\nu^2}\bigg)^{6m-5}\\
&\leqslant c_3\bigg(\bigg(\frac{N\|f\|_{-1}}{\nu^2}\bigg)^{6m-7}+\bigg(\frac{N\|f\|_{-1}}{\nu^2}\bigg)^{6m-4}+\bigg(\frac{N\|f\|_{-1}}{\nu^2}\bigg)^{6m-5}\bigg)\\
&\leqslant c_3\bigg(\frac{N\|f\|_{-1}}{\nu^2}\bigg)^{3m}\bigg(\frac{N\|f\|_{-1}}{\nu^2}\bigg)^{3m-7}\bigg(1+\bigg(\frac{N\|f\|_{-1}}{\nu^2}\bigg)^3+\bigg(\frac{N\|f\|_{-1}}{\nu^2}\bigg)^2\bigg),
\end{aligned}
$$

where

$$
c_3=\max\Big\{\frac{Nc_2\nu}{\nu-2\alpha},\frac{Nc_1\nu^2}{(\nu-2\alpha)^2},\frac{N\nu c_1}{\nu-2\alpha}\Big\}.
$$

Thanks to the assumption in this lemma, we have

$$
\|\nabla e_h^m\|\leqslant c_3\bigg(\frac{N\|f\|_{-1}}{\nu^2}\bigg)^{3m}. \tag{3.42}
$$

Now we choose

$$
c=\max\Big\{\frac{\nu\|f\|_{-1}}{(\nu-2\alpha)^2},\frac{\nu^4\|f\|_{-1}}{(\mu-2\alpha)(\nu-2\alpha)^4},\frac{\nu c_1}{\nu-2\alpha},c_3\Big\}
$$

in our proof. From (3.38) and (3.42) we know that (3.27) and (3.28) also hold for $k=m$. The proof is completed. □

**Lemma 3.3.** *Under the assumptions of Theorem* 3.2 *and Lemma* 3.2*, we have that the iteration error of pressure satisfies*

$$
\|\eta_h^m\|\leqslant c\bigg(\frac{N\|f\|_{-1}}{\nu^2}\bigg)^{3m},\quad \|\Theta_h^m\|\leqslant c\bigg(\frac{N\|f\|_{-1}}{\nu^2}\bigg)^{3m-2}.
$$

P r o o f. Using (3.21) and (3.23), we find

$$
\begin{aligned}
(\eta_h^m,\nabla\cdot v_h)&=\nu(\nabla e_h^m,\nabla-b(e_h^m,e_h^m,v_h)v_h)+G(e_h^m,v_h)+b(u_h,e_h^m,v_h)\\
&\quad+b(e_h^m,u_h,v_h)-b(E_h^{m-1}-e_h^{m-1}-E_h^m+e_h^m,E_h^m+e_h^m,v_h)\\
&\leqslant\nu\|\nabla e_h^m\|\|\nabla v_h^m\|+2\alpha\|\nabla e_h^m\|\|\nabla v_h^m\|+N(2\|\nabla u_h\|\|\nabla e_h^m\|\\
&\quad+\|\nabla e_h^m\|^2)\|\nabla v_h\|+N(\|\nabla E_h^{m-1}\|+\|\nabla e_h^{m-1}\|+\|\nabla E_h^m\|\\
&\quad+\|\nabla e_h^m\|)(\|\nabla E_h^m\|+\|\nabla e_h^m\|)\|\nabla v_h\|.
\end{aligned} \tag{3.43}
$$

With help of the discrete LBB condition (2.7), Theorem 3.1, Theorem 3.2, and Lemma 3.2, we get

$$\|\eta_h^m\| \leqslant c\bigg(\frac{N\|f\|_{-1}}{\nu^2}\bigg)^{3m}, \quad c = c(\nu, f, \beta, \alpha).$$

Using (3.22), we get

$$\begin{aligned}(3.44)\qquad (\Theta_h^m, \nabla \cdot v_h) &= \nu(\nabla E_h^m, \nabla v_h) + G(E_h^m, v_h) \\ &\quad + b(e_h^{m-1}, u_h, v_h) + b(u_h^{m-1}, E_h^m, v_h) \\ &\leqslant \nu\|\nabla E_h^m\|\|\nabla v_h\| + 2\alpha\|\nabla E_h^m\|\|\nabla v_h\| \\ &\quad + N\|\nabla e_h^{m-1}\|\|\nabla u_h\|\|\nabla v_h\| + N\|\nabla u_h^{m-1}\|\|\nabla E_h^m\|\|\nabla v_h\|.\end{aligned}$$

Applying similar techniques as above, we obtain

$$\|\Theta_h^m\| \leqslant c\bigg(\frac{N\|f\|_{-1}}{\nu^2}\bigg)^{3m-2}, \quad c = c(\nu, f, \beta, \alpha).$$

□

Finally, by using Theorem 3.1, Lemma 3.2, and Lemma 3.3, with help of the triangle inequality we get the following results.

**Theorem 3.3.** *Let the exact solution $(u, p)$ of (2.4) be in $(H^3(\Omega)^2 \cap X$, $H^2(\Omega) \cap M)$, then the solution $(u_h^m, p_h^m)$ generated by the TGEC algorithm satisfies the error estimate*

$$\|u - u_h^m\| \leqslant ch^3 + c\bigg(\frac{N\|f\|_{-1}}{\nu^2}\bigg)^{3m},$$
$$\|\nabla(u - u_h^m)\| + \|p - p_h^m\| \leqslant ch^2 + c\bigg(\frac{N\|f\|_{-1}}{\nu^2}\bigg)^{3m},$$

*and the relative coarse solution $(U_h^m, P_h^m)$ satisfies*

$$\|u - U_h^m\| \leqslant ch^2 + c\bigg(\frac{N\|f\|_{-1}}{\nu^2}\bigg)^{3m-2},$$
$$\|\nabla(u - U_h^m)\| + \|p - P_h^m\| \leqslant ch^2 + c\bigg(\frac{N\|f\|_{-1}}{\nu^2}\bigg)^{3m-2}.$$

## 4. Numerical experiments

In this section, we present numerical experiments to verify the theory analysis and illustrate the effectiveness of our method (TGEC). Here we choose Taylor-Hood FE to approximate the velocity and pressure. The code was implemented by using the public finite element software package Freefem++ [12].

The numerical examples are divided into four parts. The first part presents the rates of convergence for a smooth problem with analytical solution. The second part deals with the problem of 2D lid-driven cavity flow. We will discuss the choices of the stabilization parameter of our method, and also compare them with the benchmark data in [2]. The third part is the numerical simulation of the backward-facing step flow. We compare the numerical results with the benchmark data in [4]. Finally, the 3D lid-driven cavity model will be studied.

**4.1. Rates of convergence study.** In the first test, we consider $\Omega = [0,1]^2$. The analytical solution for the velocity $u = (u_1, u_2)$ and the pressure $p$ is given as follows:

$$u_1(x,y) = 10x^2(x-1)^2y(y-1)(2y-1),$$
$$u_2(x,y) = -10x(x-1)(2x-1)y^2(y-1)^2,$$
$$p(x,y) = 10(2x-1)(2y-1),$$

where $f(x,y) = (f_1(x,y), f_2(x,y))$ is determined by (2.1). We consider the case of viscosity $\nu = 1$, and choose $\alpha = 0.1h^2$. The experimental rates of convergence with respect to the mesh size $h$ are calculated by the formula $\log(E_i/E_{i+1})/\log(h_i/h_{i+1})$, where $E_i$ and $E_{i+1}$ are the relative errors corresponding to the mesh width $h_i$ and $h_{i+1}$, respectively. We can see from Table 1 and Figure 1 that our method confirms the convergence rates just like the theoretical analysis.

| $\frac{1}{h}$ | $\frac{\|u-u_h\|_{L^2}}{\|u\|_{L^2}}$ | $u_{L^2}$-Rate | $\frac{\|u-u_h\|_{H^1}}{\|u\|_{H^1}}$ | $u_{H^1}$-Rate | $\frac{\|p-p_h\|_{L^2}}{\|p\|_{L^2}}$ | $p_{L^2}$-Rate |
|---|---|---|---|---|---|---|
| 4 | 0.0402779 | | 0.164769 | | 0.0485817 | |
| 8 | 0.00493378 | 3.02922 | 0.0442181 | 1.89774 | 0.0121142 | 2.00372 |
| 12 | 0.00144403 | 3.03026 | 0.0199874 | 1.95833 | 0.00538951 | 1.99751 |
| 16 | 0.000611914 | 2.98455 | 0.0113183 | 1.97676 | 0.00304275 | 1.98724 |
| 20 | 0.000322583 | 2.86915 | 0.00726897 | 1.98441 | 0.00196265 | 1.96494 |

Table 1. Rates of convergence using TGEC algorithm.

**4.2. The 2D lid-driven cavity flow.** The 2D lid-driven cavity flow is a popular benchmark problem for testing the numerical schemes of incompressible flow, which has been analyzed in [5] and [2]. In this problem, computations are carried out in

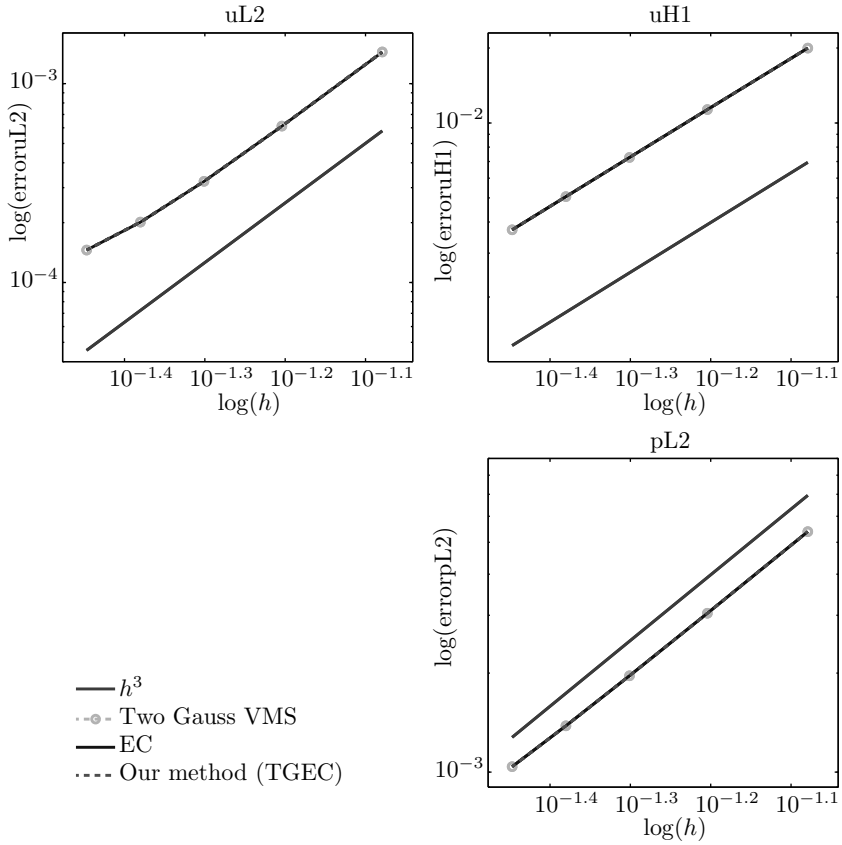


Figure 1. Convergence analysis for the velocity and pressure. Left: $L^2$-error for the velocity; right: $H^1$-error for the velocity; lower right: $L^2$-error for the pressure.

the domain $\Omega = (0,1)^2$. The flow is driven by the tangential velocity field on the top boundary in the absence of other body forces. For more detailed information, we can see Figure 2. The presented numerical results are compared with the benchmark data of Erturk et al. [2].

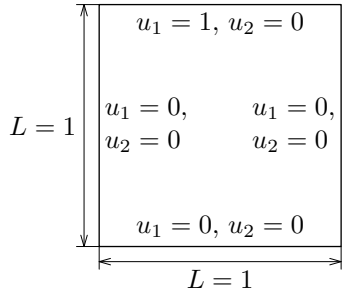


Figure 2. Schematic diagram of the lid-driven cavity flow.

We first study how to choose a best stabilization parameter in the computation. We test Reynolds numbers (Re = 1000, 3200, 5000, 7500, 10000, 12500, 15000, 17500) corresponding to the mesh width ($h = 1/24$, $1/32$, $1/48$, $1/64$, $1/84$, $1/90$, $1/100$, $1/125$). From Tables 2 and 3 (the symbol '–' denotes divergence, the same as below), we can find that the stabilization parameter has a close relationship with the Reynolds number and the mesh width. With the decrease of the mesh width, while $\mathrm{Re} < 10000$, $\alpha = \nu h$ is the best choice, since both the CPU time and the iterations are smallest relatively. While $\mathrm{Re} \geqslant 10000$, $\alpha = 0.1h^2$ is the best choice, because both the CPU time and the iterations are smallest relatively. We can find $\alpha = 0.1h$ is the worst choice in our method.

| Re | 1000 | 3200 | 5000 | 7500 | 10000 | 12500 | 15000 | 17500 |
|---|---|---|---|---|---|---|---|---|
| $h$ | $\frac{1}{24}$ | $\frac{1}{32}$ | $\frac{1}{48}$ | $\frac{1}{64}$ | $\frac{1}{84}$ | $\frac{1}{90}$ | $\frac{1}{100}$ | $\frac{1}{125}$ |
| $\alpha = 0.1h$ | 122.83 | 1318.33 | – | – | – | – | – | – |
| $\alpha = \nu h$ | 17.34 | 53.375 | 129.14 | 348.33 | – | – | – | – |
| $\alpha = 0.1h^2$ | 23.30 | 60.73 | 159.10 | 463.45 | 620.77 | 863.44 | 745.10 | 1745.16 |

Table 2. CPU time at different stabilization parameters.

| Re | 1000 | 3200 | 5000 | 7500 | 10000 | 12500 | 15000 | 17500 |
|---|---|---|---|---|---|---|---|---|
| $h$ | $\frac{1}{24}$ | $\frac{1}{32}$ | $\frac{1}{48}$ | $\frac{1}{64}$ | $\frac{1}{84}$ | $\frac{1}{90}$ | $\frac{1}{100}$ | $\frac{1}{125}$ |
| $\alpha = 0.1h$ | 68 | 154 | – | – | – | – | – | – |
| $\alpha = \nu h$ | 9 | 17 | 17 | 27 | – | – | – | – |
| $\alpha = 0.1h^2$ | 12 | 19 | 19 | 23 | 21 | 38 | 26 | 26 |

Table 3. Iterations at different stabilization parameters.

Next, in order to show the stability and high efficiency of our method, we present the velocity streamlines and the pressure contours in Figures 3–5. In addition, we draw the horizontal velocity ($u_1$-velocity) along the vertical centerline and the vertical velocity ($u_2$-velocity) along the horizontal centerlines, and compare them with those of Erturk et al. [2] at Re = 10000, 15000, and 17500, respectively. Noting that the benchmark data of Erturk et al. [2] were computed on a much finer $601 \times 601$ grid mesh, Figures 6–8 show the accuracy of TGEC algorithm.

**4.3. Backward-facing step flow.** To show the stability and efficiency of our method, we test another benchmark problem, the backward-facing step flow model, which has been analyzed in [4]. The problem is defined on a long channel $[0, 30] \times [-0.5, 0.5]$ with no-slip conditions on the top and bottom walls, as well as on the lower half part of the left wall. The parabolic horizontal component of velocity is given by $u_1 = 24y(0.5 - y)$ for $0 \leqslant y \leqslant 0.5$ at the inlet boundary, and the outlet boundary

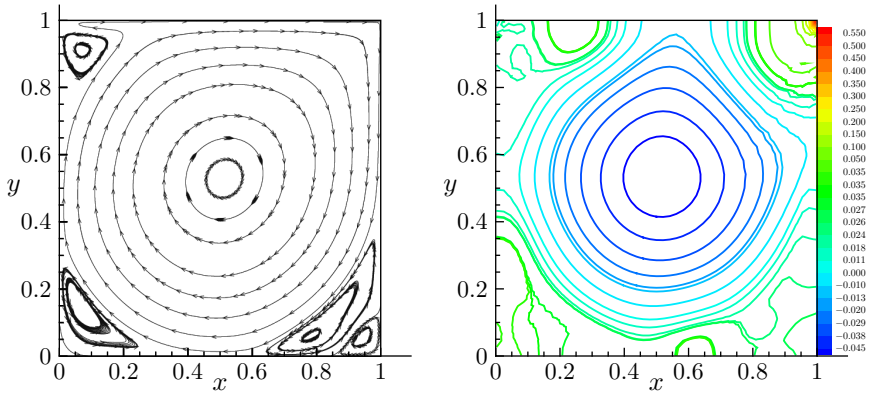


(a) Streamline (b) Pressure

Figure 3. Contour lines of the streamline and pressure with Re = 10000.

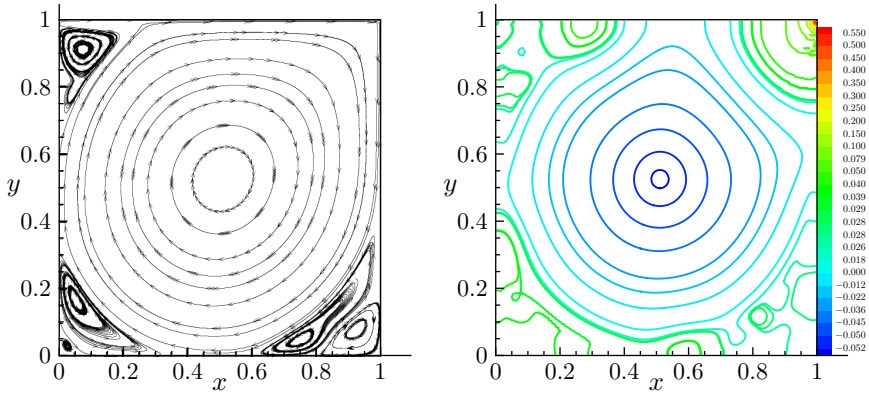


(a) Streamline (b) Pressure

Figure 4. Contour lines of the streamline and pressure with Re = 15000.

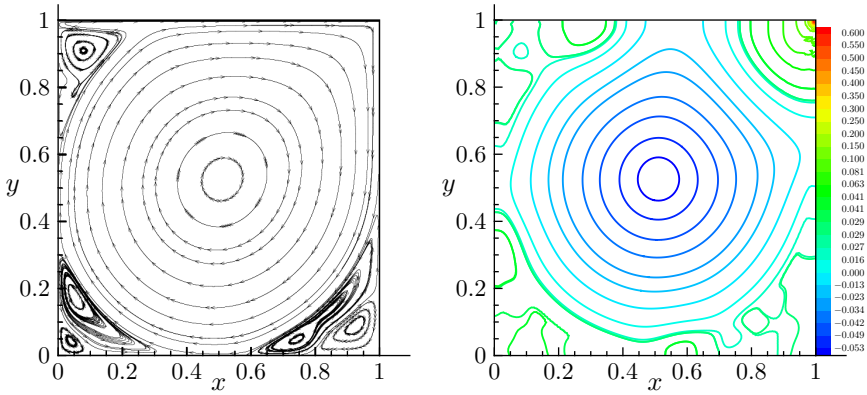


(a) Streamline (b) Pressure

Figure 5. Contour lines of the streamline and pressure with Re = 17500.

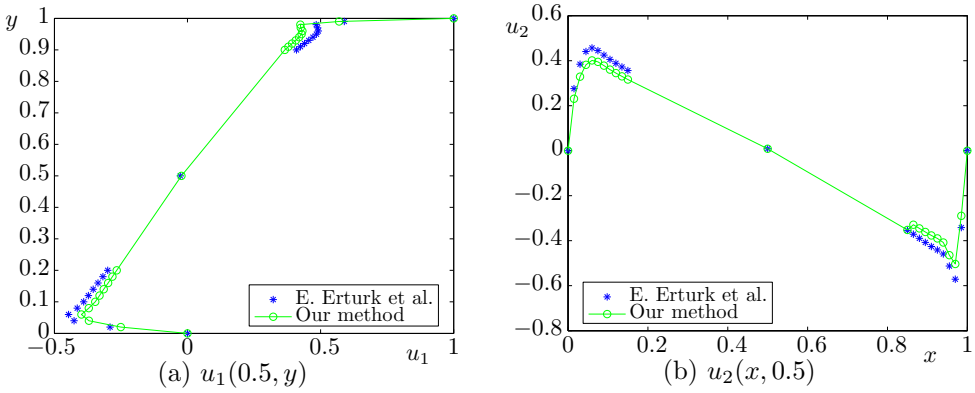


(a) $u_1(0.5, y)$ (b) $u_2(x, 0.5)$

Figure 6. The $u_1$-velocity at vertical centerline (left) and the $u_2$-velocity at horizontal centerline (right) for Re = 10000.

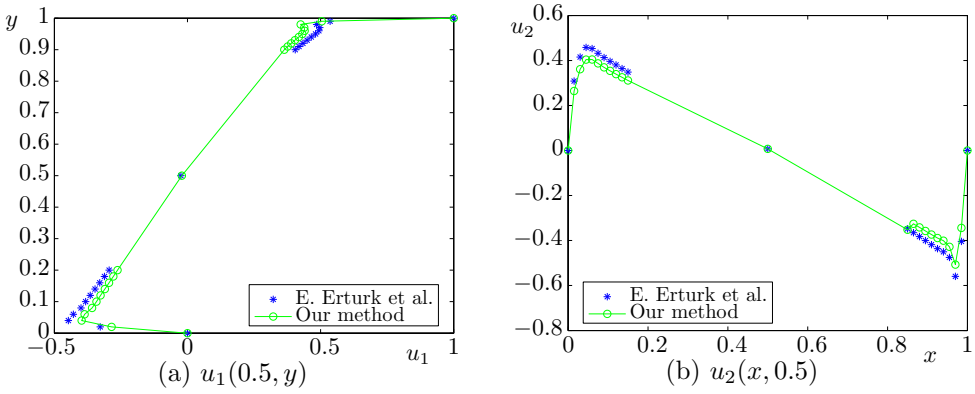


(a) $u_1(0.5, y)$ (b) $u_2(x, 0.5)$

Figure 7. The $u_1$-velocity at vertical centerline (left) and the $u_2$-velocity at horizontal centerline (right) for Re = 15000.

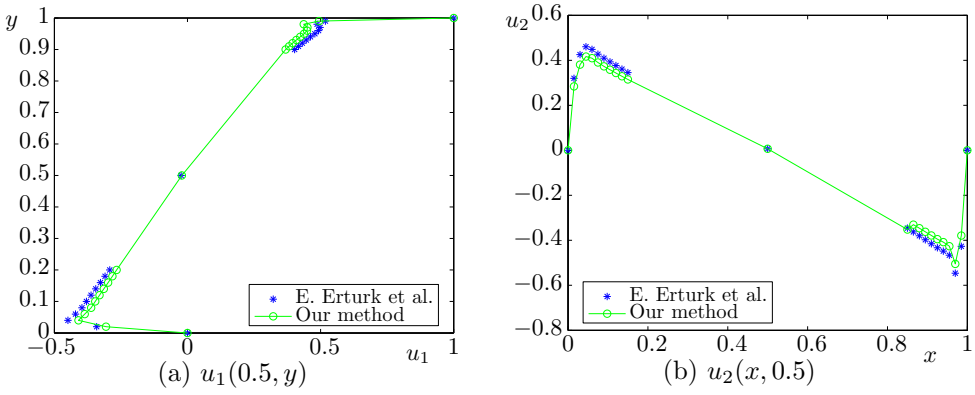


(a) $u_1(0.5, y)$ (b) $u_2(x, 0.5)$

Figure 8. The $u_1$-velocity at vertical centerline (left) and the $u_2$-velocity at horizontal centerline (right) for Re = 17500.

condition is set as $-p + \nu\partial u_1/\partial x = 0$, $u_2 = 0$. For more detailed information, see Figure 9. The Reynolds number for this problem is defined as $\mathrm{Re} = u_{\mathrm{ave}}H/\nu$, where $u_{\mathrm{ave}} = 1$ is the average velocity at the inlet boundary and $L = 1$ is the channel height.

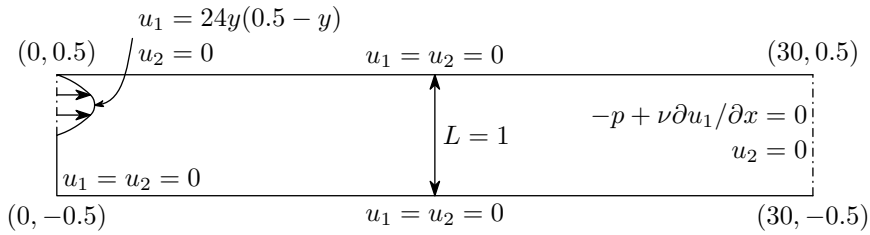


Figure 9. Schematic diagram of the backward-facing step flow.

We set the mesh size $h = 1/30$ and $\alpha = 0.1h^2$. We first compute an approximate solution at $\mathrm{Re} = 800$ by using our method TGEC, and then compare the computed velocity and pressure across the channel at $x = 7$ and $x = 15$ with those of Gartling [4]. From Figure 10 we can see that our numerical results coincide well with those of Gartling [4]. Figure 11 describes the computed pressure and shear stress along the upper and lower channel walls, which are also consistent with those of [4]. The numerical results illustrate the effectiveness of the method.

**4.4. The 3D lid-driven cavity flow.** Our final numerical example is the 3D lid-driven cavity flow problem, which is tested in [27]. The domain of this problem is the unit cube $[0, 1]^3$, equipped with horizontal velocity as boundary conditions for the top face ($z = 1$) and homogeneous Dirichlet boundary conditions on the other faces. We implement our method (TGEC) with the mesh width $h = 1/8$, the stabilization parameter $\alpha = 0.1h^2$.

In Figure 12, we draw the centerline $x$-velocity at $\mathrm{Re} = 100, 400$, and 1000, respectively, comparing it with the reference values given by Wone and Baker [27]. Figures 13–15 plot the mid-plane velocity streamline pictures for $\mathrm{Re} = 100, 400$ and 1000, respectively, which illustrates the effectiveness of our proposed method. All these numerical results are in good agreement with the reference solution in [27].

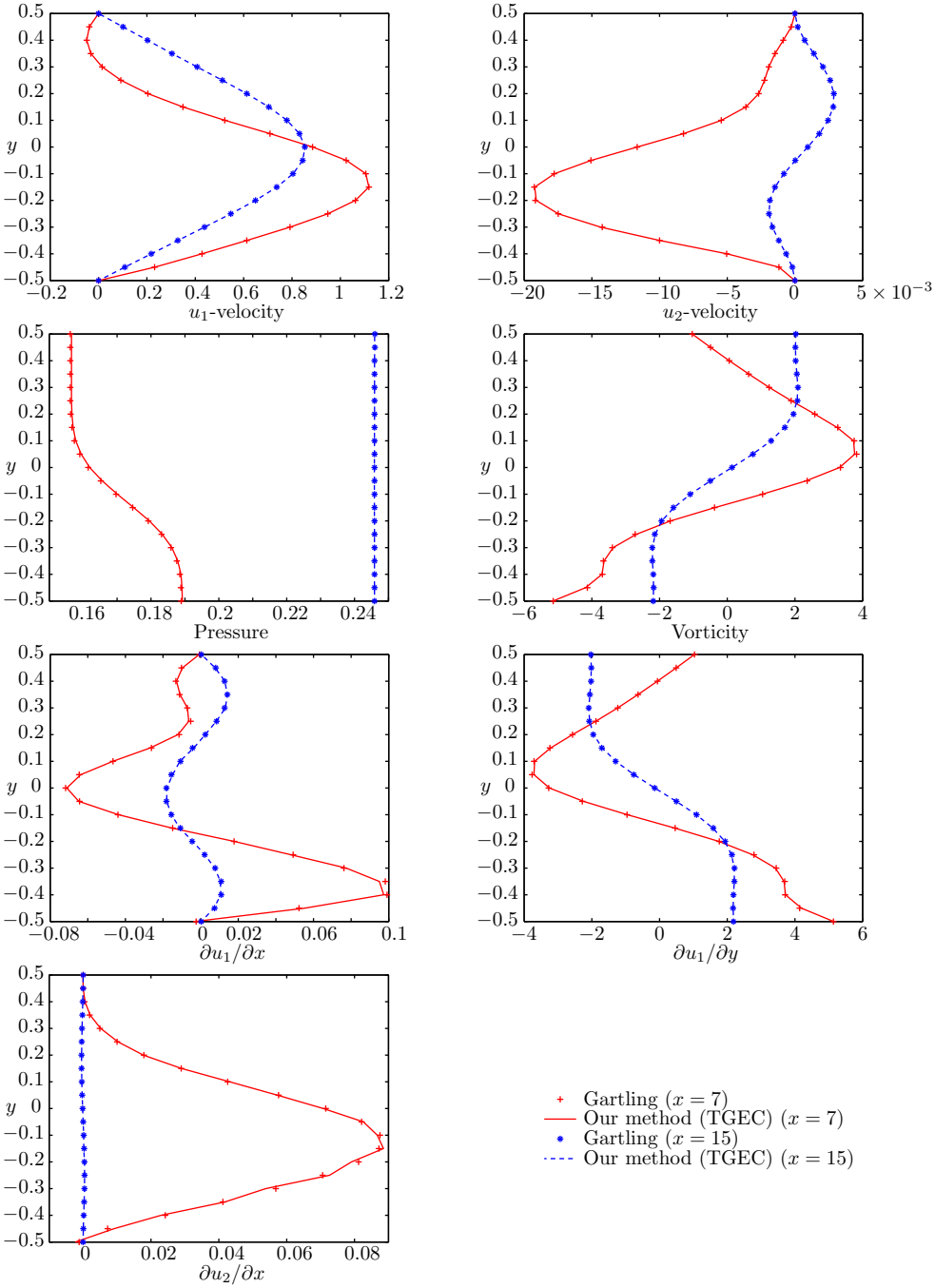


Figure 10. Comparison of $u_1$, $u_2$, $p$, $w = \partial u_2/\partial x - \partial u_1/\partial y$, $\partial u_1/\partial x$, $\partial u_1/\partial y$, $\partial u_2/\partial x$ (from top to bottom, left to right); profiles at different locations for backward-facing step flow at $\mathrm{Re} = 800$.

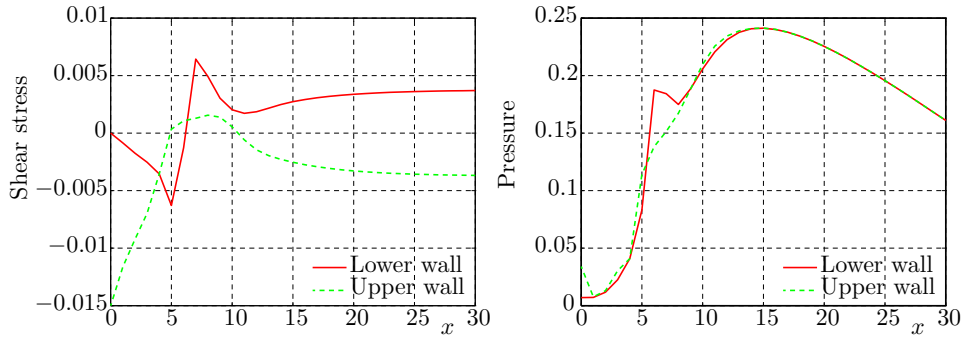


Figure 11. Shear stress profile (left) and pressure profiles (right) along the upper and lower channel walls for the backward-facing step flow at Re = 800.

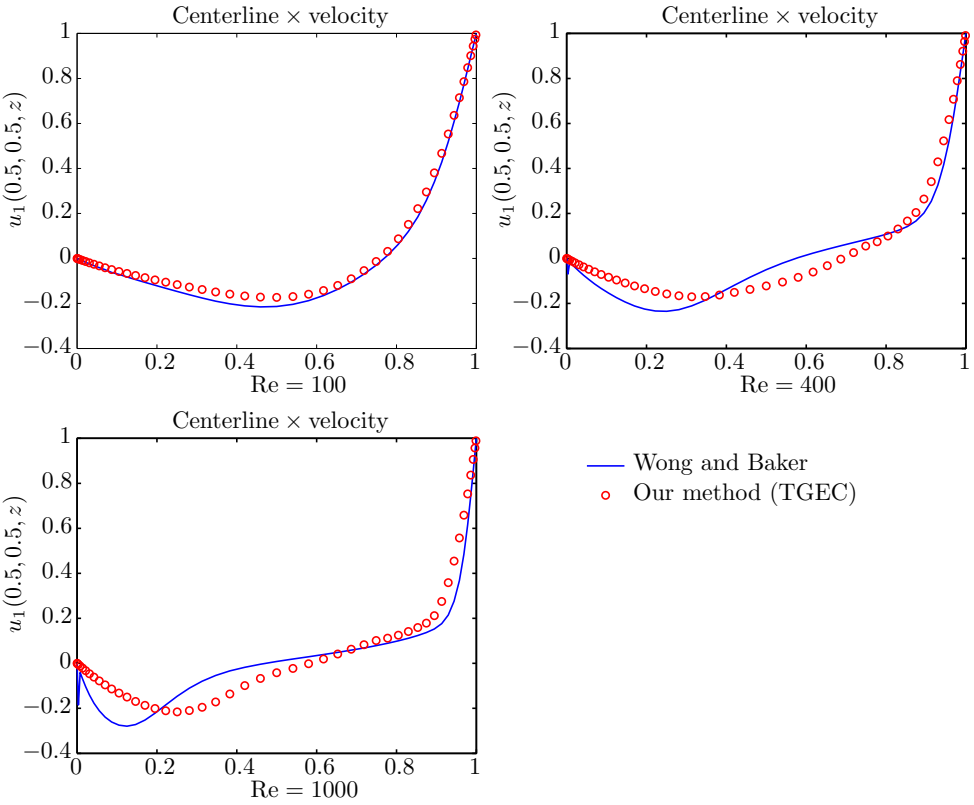


Figure 12. The centerline $x$-velocities of the 3D lid-driven cavity flow at Re = 100, 400, and 1000.

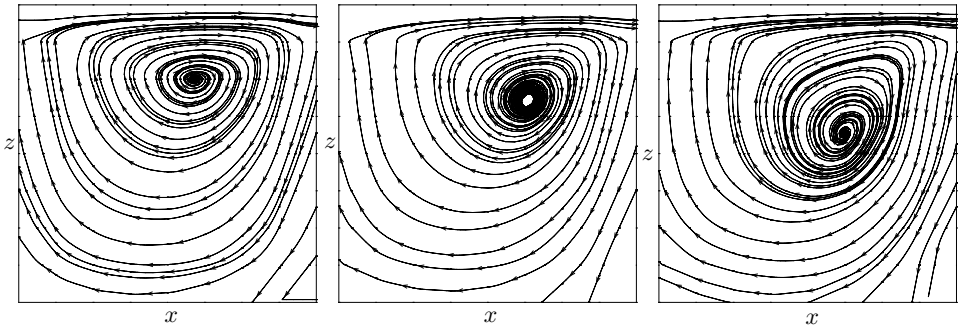


Figure 13. The $xz$-plane velocity streamline pictures of the 3D lid-driven cavity flow at $y = 0.5$: Re $= 100, 400$, and 1000 (from left to right).

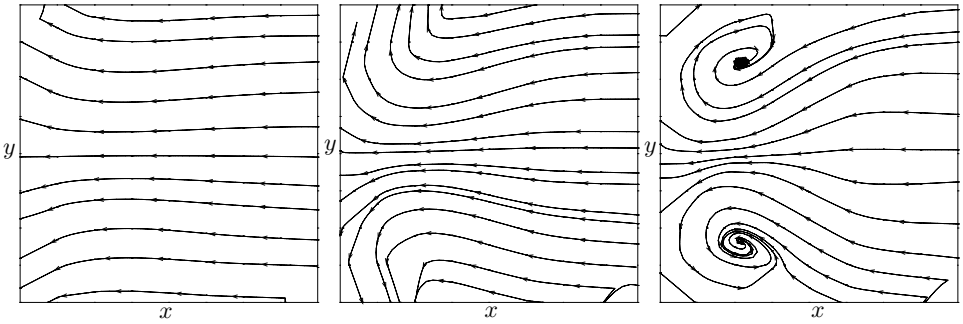


Figure 14. The $xy$-plane velocity streamline pictures of the 3D lid-driven cavity flow at $z = 0.5$: Re $= 100, 400$, and 1000 (from left to right).

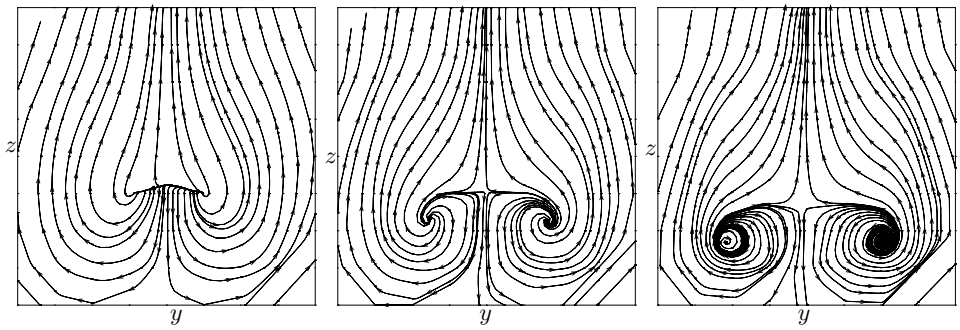


Figure 15. The $yz$-plane velocity streamline pictures of the 3D lid-driven cavity flow at $x = 0.5$: Re $= 100, 400$, and 1000 (from left to right).

## 5. Conclusions

A new finite element error correction method based on two local Gauss integrations (TGEC) for the Navier-Stokes equations has been proposed and analyzed in this article. This method possesses the advantages of both the EC and TGVMS methods, which makes it very efficient in solving the Navier-Stokes equations at high Reynolds number. Stability and error analysis of this method is given. Numerical tests verified the theoretical preconditions and demonstrated the effectiveness of the method. The application of the method to 3D coupled fluid flows simulation problem and the combination with the two-level method will be considered in the future.

*References*


[1] *S. C. Brenner, L. R. Scott*: The Mathematical Theory of Finite Element Methods. Texts in Applied Mathematics 15, Springer, New York, 2008. zbl MR doi

[2] *E. Erturk, T. C. Corke, C. Gökçöl*: Numerical solutions of 2-D steady incompressible driven cavity flow at high Reynolds numbers. Int. J. Numer. Methods Fluids *48* (2005), 747–774. zbl doi

[3] *V. J. Ervin, W. J. Layton, J. M. Maubach*: Adaptive defect-correction methods for viscous incompressible flow problems. SIAM J. Numer. Anal. *37* (2000), 1165–1185. zbl MR doi

[4] *D. K. Gartling*: A test problem for outflow boundary conditions—flow over a backward-facing step. Int. J. Numer. Methods Fluids *11* (1990), 953–967. doi

[5] *U. Ghia, K. N. Ghia, C. T. Shin*: High-Re solutions for incompressible flow using the Navier-Stokes equations and a multigrid method. J. Comput. Phys. *48* (1982), 387–411. zbl doi

[6] *V. Girault, P.-A. Raviart*: Finite Element Methods for Navier-Stokes Equations. Theory and Algorithms. Springer Series in Computational Mathematics 5, Springer, Berlin, 1986. zbl MR doi

[7] *P. M. Gresho, R. L. Lee, S. T. Chan, R. L. Sani*: Solution of the time-dependent incompressible Navier-Stokes and Boussinesq equations using the Galerkin finite element method. Approximation Methods for Navier-Stokes Problems, Proc. Symp. IUTAM, Paderborn 1979. Lect. Notes in Math. 771, Springer, Berlin, 1980, pp. 203–222. zbl MR doi

[8] *J.-L. Guermond, A. Marra, L. Quartapelle*: Subgrid stabilized projection method for 2D unsteady flows at high Reynolds numbers. Comput. Methods Appl. Mech. Eng. *195* (2006), 5857–5876. zbl MR doi

[9] *M. D. Gunzburger*: Finite Element Methods for Viscous Incompressible Flows. A Guide to Theory, Practice, and Algorithms. Computer Science and Scientific Computing, Academic Press, Boston, 1989. zbl MR

[10] *Y. He, J. Li*: Convergence of three iterative methods based on the finite element discretization for the stationary Navier-Stokes equations. Comput. Methods Appl. Mech. Eng. *198* (2009), 1351–1359. zbl MR doi

[11] *Y. He, A. Wang, L. Mei*: Stabilized finite-element method for the stationary Navier-Stokes equations. J. Eng. Math. *51* (2005), 367–380. zbl MR doi

[12] *F. Hecht*: New development in freefem++. J. Numer. Math. *20* (2012), 251–265. zbl MR doi

[13] *P. Huang, X. Feng, Y. He*: Two-level defect-correction Oseen iterative stabilized finite element methods for the stationary Navier-Stokes equations. Appl. Math. Modelling *37* (2013), 728–741. MR doi

[14] *P. Huang, Y. He, X. Feng*: A new defect-correction method for the stationary Navier-Stokes equations based on local Gauss integration. Math. Methods Appl. Sci. *35* (2012), 1033–1046. zbl MR doi
[15] *T. J. R. Hughes, L. Mazzei, K. E. Jansen*: Large eddy simulation and the variational multiscale method. Comput. Vis. Sci. *3* (2000), 47–59. zbl doi
[16] *V. John, S. Kaya*: A finite element variational multiscale method for the Navier-Stokes equations. SIAM J. Sci. Comput. *26* (2005), 1485–1503. zbl MR doi
[17] *S. Kaya, B. Rivière*: A two-grid stabilization method for solving the steady-state Navier-Stokes equations. Numer. Methods Partial Differ. Equations *22* (2006), 728–743. zbl MR doi
[18] *A. Labovschii*: A defect correction method for the time-dependent Navier-Stokes equations. Numer. Methods Partial Differ. Equations *25* (2009), 1–25. zbl MR doi
[19] *W. Layton*: A connection between subgrid scale eddy viscosity and mixed methods. Appl. Math. Comput. *133* (2002), 147–157. zbl MR doi
[20] *W. Layton, H. K. Lee, J. Peterson*: A defect-correction method for the incompressible Navier-Stokes equations. Appl. Math. Comput. *129* (2002), 1–19. zbl MR doi
[21] *J. Li, Y. He*: A stabilized finite element method based on two local Gauss integrations for the Stokes equations. J. Comput. Appl. Math. *214* (2008), 58–65. zbl MR doi
[22] *Y. Li, L. Mei, Y. Li, K. Zhao*: A two-level variational multiscale method for incompressible flows based on two local Gauss integrations. Numer. Methods Partial Differ. Equations *29* (2013), 1986–2003. zbl MR doi
[23] *Q. Liu, Y. Hou*: A two-level defect-correction method for Navier-Stokes equations. Bull. Aust. Math. Soc. *81* (2010), 442–454. zbl MR doi
[24] *H. G. Melhem*: Finite element approximation to heat transfer through construction glass blocks. Mechanics Computing in 1990's and Beyond. American Society of Civil Engineers, 1991, pp. 193–197.
[25] *R. Temam*: Navier-Stokes Equations. Theory and Numerical Analysis. Studies in Mathematics and Its Applications 2, North-Holland, Amsterdam, 1984. zbl MR
[26] *K. Wang, Y. S. Wong*: Error correction method for Navier-Stokes equations at high Reynolds numbers. J. Comput. Phys. *255* (2013), 245–265. MR doi
[27] *K. L. Wong, A. J. Baker*: A 3D incompressible Navier-Stokes velocity-vorticity weak form finite element algorithm. Int. J. Numer. Methods Fluids *38* (2002), 99–123. zbl doi
[28] *H. Zheng, Y. Hou, F. Shi, L. Song*: A finite element variational multiscale method for incompressible flows based on two local Gauss integrations. J. Comput. Phys. *228* (2009), 5961–5977. MR zbl doi
[29] *O. C. Zienkiewicz, R. L. Taylor*: The Finite Element Method for Solid and Structural Mechanics. Elsevier/Butterworth Heinemann, Amsterdam, 2005. zbl doi

*Authors' addresses*: *Yun-Bo Yang*, School of Mathematics and Statistics, Xi'an Jiaotong University, Xi'an, Shaanxi, 710049, P. R. China, e-mail: `yangyunbo@stu.xjtu.edu.cn`; *Qiong-Xiang Kong* (corresponding author), School of Human Settlements and Civil Engineering, Xi'an Jiaotong University, Xi'an, Shaanxi, 710049, P. R. China, e-mail: `qxkong@mail.xjtu.edu.cn`.